

Chloride as tracer of solute transport in the aquifer–aquitard system in the Pearl River Delta, China

Xingxing Kuang¹ · Jiu Jimmy Jiao¹ · Ya Wang²

Received: 6 August 2015 / Accepted: 14 January 2016 / Published online: 4 February 2016
© Springer-Verlag Berlin Heidelberg 2016

Abstract A 1D numerical model is constructed to investigate the impact of sedimentation and sea level changes on transport of Cl^- in the aquifer–aquitard system in the Pearl River Delta (PRD), China. The model simulates the evolution of the vertical Cl^- concentration profiles during the Holocene. Sedimentation is modeled as a moving boundary problem. Chloride concentration profiles are reconstructed for nine boreholes, covering a wide area of the PRD, from northwest to southeast. Satisfactory agreement is obtained between simulated and measured Cl^- concentration profiles. Diffusion solely is adequate to reproduce the vertical Cl^- concentration profiles, which indicates that diffusion is the regionally dominant vertical transport mechanism across the aquitards in the PRD. The estimated effective diffusion coefficients of the aquitards range from 2.0×10^{-11} to 2.0×10^{-10} m^2/s . The effective diffusion coefficients of the aquifers range from 3.0×10^{-11} to 4.0×10^{-10} m^2/s . Advective transport tends to underestimate Cl^- concentrations in the aquitard and overestimate Cl^- concentrations in the basal aquifer. The results of this study will help understand the mechanisms of solute transport in the PRD and other deltas with similar geological and hydrogeological characteristics.

Keywords Chloride · Sedimentation · Solute transport · Numerical modeling · China

✉ Jiu Jimmy Jiao
jjiao@hku.hk

¹ Department of Earth Sciences, The University of Hong Kong, Pokfulam Road, Hong Kong, China

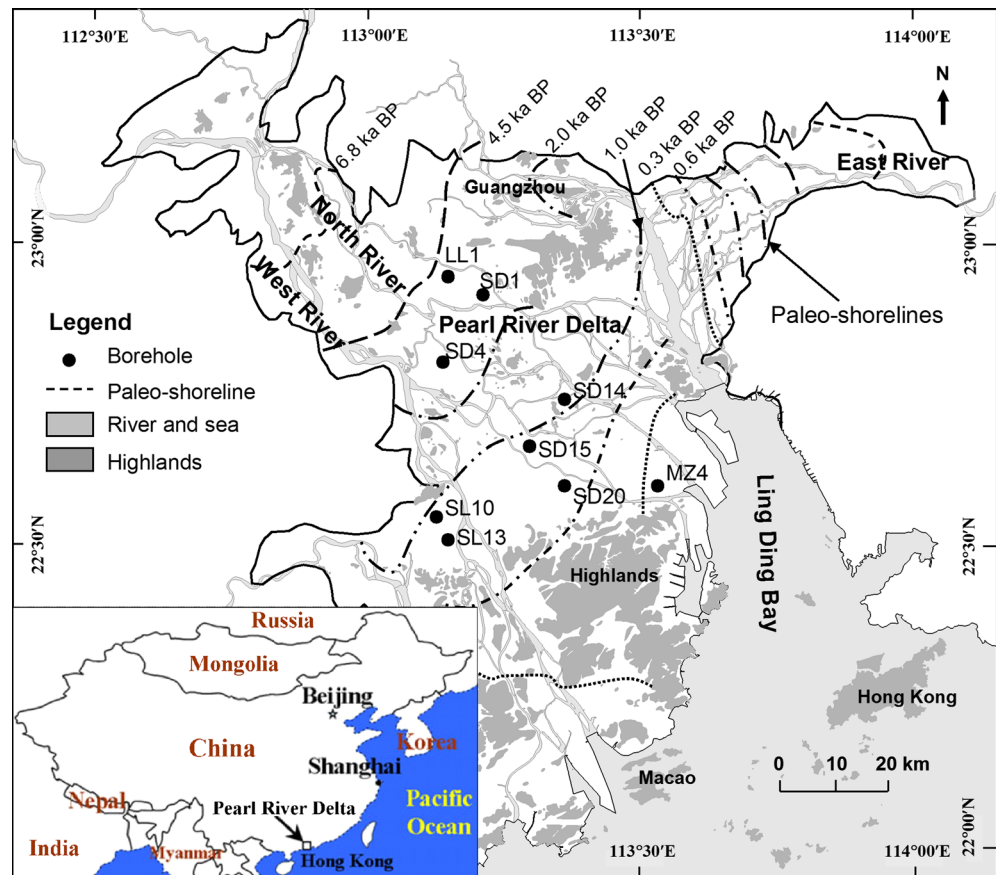
² School of Earth Science and Geological Engineering, Sun Yat-Sen University, Guangzhou 510275, China

Introduction

Sedimentation has been found to have an important impact on the transport of chloride (Cl^-) in porous media, especially in low-permeability sediment such as silt and clay (Beekman 1991; Beekman et al. 2011). Numerical simulations show that the shapes of the modeled Cl^- concentration profiles are controlled by sedimentation and Cl^- concentration at the upper boundary (Jiao et al. 2015; Kuang et al. 2015). Although sedimentation is very important to the transport of Cl^- in Quaternary sediment, numerical studies on Cl^- transport with sedimentation included are limited (Beekman 1991; Beekman et al. 2011; Tokunaga et al. 2011; Jiao et al. 2015; Kuang et al. 2015). Beekman (1991) and Beekman et al. (2011) used the numerical model EMSD (Erosion-Mixing-Sedimentation-Diffusion) to investigate the Cl^- transport mechanisms in sediment from a former brackish lagoon in the Netherlands. Tokunaga et al. (2011) simulated the Cl^- concentration profile in a coastal area in Japan. Jiao et al. (2015) reconstructed the historical conservative transport of pore-water Cl^- concentration profile in sediment below the seabed in Hong Kong, China. Researchers (Middelburg and de Lange 1989; Eggenkamp 1994; Eggenkamp et al. 1994; Groen et al. 2000) also used the analytical solution derived by Ogata and Banks (1961) to reconstruct the Cl^- concentration profile.

The Pearl River Delta (PRD) is located in the southern part of China (Fig. 1). The Quaternary stratigraphy of the PRD is characterized by an aquifer–aquitard system with laterally extensive aquitards. The aquifer–aquitard system in the PRD has been found to have abnormally high concentrations of ammonium (Jiao et al. 2010). Elevated concentrations of arsenic have also been identified in the confined basal aquifer underlying the aquitard (Wang et al. 2012). Studies have been conducted

Fig. 1 Locations of the boreholes and the paleo-shorelines in the PRD. The *inset* map, showing the location of the PRD, was modified from Wang et al. (2013a). The paleo-shorelines were obtained based on Li and Qiao (1982), Li et al. (1991), and Zong et al. (2009a)



to investigate the hydrogeochemical characteristics of the aquifer–aquitard system in the PRD (Wang and Jiao 2012; Wang et al. 2013b).

Studies on solute transport in the aquifer–aquitard system in the PRD are very limited (Wang et al. 2013a; Kuang et al. 2015). Using a one-dimensional (1D) numerical model with MODFLOW-96 (McDonald and Harbaugh 1988; Harbaugh and McDonald 1996) and MT3D (Zheng 1990), Wang et al. (2013a) simulated the salinity profiles of two boreholes. Sedimentation was simulated by three separated sub-models at different times. Kuang et al. (2015) constructed a 1D numerical model to investigate the vertical transport mechanisms of Cl^- , $\delta^2\text{H}$ and $\delta^{18}\text{O}$ in a borehole in the PRD. The continuous sedimentation process was included in the model as a moving upper boundary. There have been no published studies on the regional vertical transport mechanisms of Cl^- across the PRD.

The aim of this study is to investigate how the Cl^- concentration in the aquifer–aquitard system is controlled by sedimentation and sea level changes. Measured Cl^- concentration profiles of nine boreholes across the PRD will be used to systematically investigate the vertical transport mechanisms of Cl^- in the aquifer–aquitard system.

Study area

The Quaternary sediment in the PRD consists mainly of two terrestrial units and two marine units. The two terrestrial units are called T1 and T2 and the two marine units are called M1 and M2 (Zong et al. 2009b). From young to old, the stratigraphic sequence in the PRD is M1, T1, M2, and T2. The oldest unit T2 (sand and gravel) was deposited in a number of paleo-valleys before the last transgression in the late Pleistocene—Marine Isotope Stage (MIS) 5. The older marine unit M2 (silt and clay) was deposited during the last interglacial period. During the last glacial period (MIS 4-2), the sea level regressed and the upper part of M2 was subaerially exposed and weathered (Zong et al. 2009b). During the same period, the younger terrestrial unit T1 (alluvial sand and gravel) was deposited along paleo-river channels. In the early Holocene, the rapid rise in sea level caused widespread marine inundation and sedimentation. The youngest unit M1 (silt and clay) was deposited as a result of the rapid sea level rise. In many places, M2 and T1 are missing (Jiao et al. 2010). M1 and M2 are aquitards and T1 and T2 are aquifers. T2 is the basal confined aquifer.

The Quaternary stratigraphy of the PRD is dominated by the two areally extensive clay-rich aquitards (Zong et al. 2009b;

Jiao et al. 2010; Wang and Jiao 2012; Wang et al. 2013b). The two aquitards are characterized by very low hydraulic conductivity. The vertical hydraulic conductivity of the soft soil in the PRD with depth ranges from 2.4 to 12 m below ground surface was found to range from 10^{-10} to 10^{-8} m/s (Chen et al. 2003). On the basis of slug test analysis, researchers found that the horizontal hydraulic conductivity of the aquitards ranges from 2.2×10^{-10} to 8.2×10^{-9} m/s (Jiao et al. 2010; Wang et al. 2013a; Yang et al. 2015). The vertical hydraulic conductivity is expected to be even lower (Jiao et al. 2010). The bedrock underlying the Quaternary sediment in the PRD consists of a series of Tertiary red continental clastic rocks such as siltstone and mudstone (Huang et al. 1982; Long 1997). The hydraulic conductivity of the bedrock is considered to be much lower than the overlying unit T2 (Wang et al. 2013a). The topography of the PRD is very gentle and the water table is shallow everywhere, suggesting sluggish regional flow towards the coastline (Jiao et al. 2010; Wang et al. 2012). The regional groundwater flow in the basal aquifer (T2) in the PRD is stagnant and paleo-seawater originated from Holocene transgression is still trapped in this unit (Wang et al. 2012).

A total of nine boreholes (MZ4, SD1, SD4, SD14, SD15, SD20, LL1, SL10, and SL13) with measured Cl^- concentration profiles were used in this study (Fig. 1). The locations of the boreholes were obtained from Jiao et al. (2010) and Wang and Jiao (2012). The boreholes cover a wide area of the PRD, from northwest to southeast. The borehole depths and stratigraphic units were obtained based on previous studies (Jiao et al. 2010; Wang 2011; Zong et al. 2012; Wang et al. 2013a, b), as shown in Fig. 2. For most of the boreholes, there are only two stratigraphic units, with M1 overlying T2. Only two boreholes (SD14 and SD15) have unit M2 and only one borehole (SD15) has all four stratigraphic units.

Numerical simulation

Mathematical model

In aquifer–aquitard systems dominated by areally extensive aquitards, a 1D model has generally been used to simulate Cl^- transport (Desaulniers et al. 1981, 1986; Desaulniers and Cherry 1989; Johnson et al. 1989; Hendry et al. 2000; Beekman et al. 2011; Tokunaga et al. 2011; Kuang et al. 2015). The governing equation for 1D Cl^- transport in the aquifer–aquitard system of the PRD can be written as (Zheng and Bennett 2002)

$$\frac{\partial}{\partial z} \left(\phi D \frac{\partial C}{\partial z} \right) - \frac{\partial (v\phi C)}{\partial z} = \phi \frac{\partial C}{\partial t} \quad (1)$$

where C is the Cl^- concentration, D is the coefficient of hydrodynamic dispersion, v is the average linear pore-water

velocity in the vertical direction, ϕ is the porosity of the porous medium, z is the depth, and t is time. The coefficient of hydrodynamic dispersion is defined as $D = D_e + \alpha v$, where D_e is the effective diffusion coefficient and α is the dispersivity of the porous medium. The quantity v is defined as $v = q/\phi_e$, where q is the Darcy velocity and ϕ_e is the effective porosity. The effective porosity was assumed to be equal to the porosity, i.e., $\phi_e = \phi$ (van der Kamp et al. 1996; Hendry and Wassenaar 1999). The porosities of the aquifer and the aquitard were set to be 0.3 (Jiao et al. 2010; Wang et al. 2013a) and 0.5 (Fetter 2001), respectively. Advection in the aquifer–aquitard system was assumed to follow Darcy's law and there is no threshold hydraulic gradient (Neuzil 1986). According to previous studies (Beekman et al. 2011; Tokunaga et al. 2011; Wang et al. 2013a; Kuang et al. 2015), compaction-driven flow was ignored. In addition, the aquifer and the aquitard were assumed to be individually homogeneous.

The upper boundary of the model locates at the surface of M1, which is the sediment–water interface. It is very important to determine the sea level changes in the Holocene because M1 is deposited during this period (Zong et al. 2009a, b). Sea level changes in the PRD have been extensively studied (Yang and Xie 1985; Li et al. 1991; Long 1997; Zong 2004). Some researchers presented comparisons of these sea level curves (Long 1997; Wang 2011; Wei and Wu 2011). A simplified sea level curve used herein is shown in Fig. 3a. The sea level at 10 thousand calendar years before present (ka BP) has been found to range from 30 m to over 100 m below present. Then the sea level rose rapidly and reached the present level at about 6 ka BP (Chen et al. 1990; Zong 2004; Yim et al. 2006; Wu et al. 2007; Wei and Wu 2011; Zong et al. 2012). The sea level remained relatively stable after 6 ka BP (Wu et al. 2007; Wei and Wu 2011). Monsoonal discharge became one of the dominant mechanisms for sedimentation in the PRD (Zong et al. 2009a). The paleo-shoreline positions are obtained from the literature (Li and Qiao 1982; Li et al. 1991; Zong et al. 2009a), as shown in Fig. 1.

The upper boundary is a moving boundary with the moving rate equal to the sedimentation rate (Beekman et al. 2011; Tokunaga et al. 2011; Jiao et al. 2015; Kuang et al. 2015). Downward diffusion of Cl^- and sedimentation were assumed to occur simultaneously (Tokunaga et al. 2011; Jiao et al. 2015; Kuang et al. 2015). The model begins at the beginning of the deposition of M1 and stops at present time. Previous studies show that the time when M1 began to deposit is approximately 10 ka BP (Lan 1991; Zong et al. 2012; Wang et al. 2013a). On the basis of the changes of the simplified sea level (Fig. 3a), the changes of Cl^- concentration at the upper boundary with time during the last 10 ka can be divided into three periods (Kuang et al. 2015), namely the marine period from 0 to t_1 , the transition period from t_1 to t_2 , and the terrestrial period from t_2 to t_3 . The time $t = 0$ represents the time when M1 began to deposit (10 ka BP).

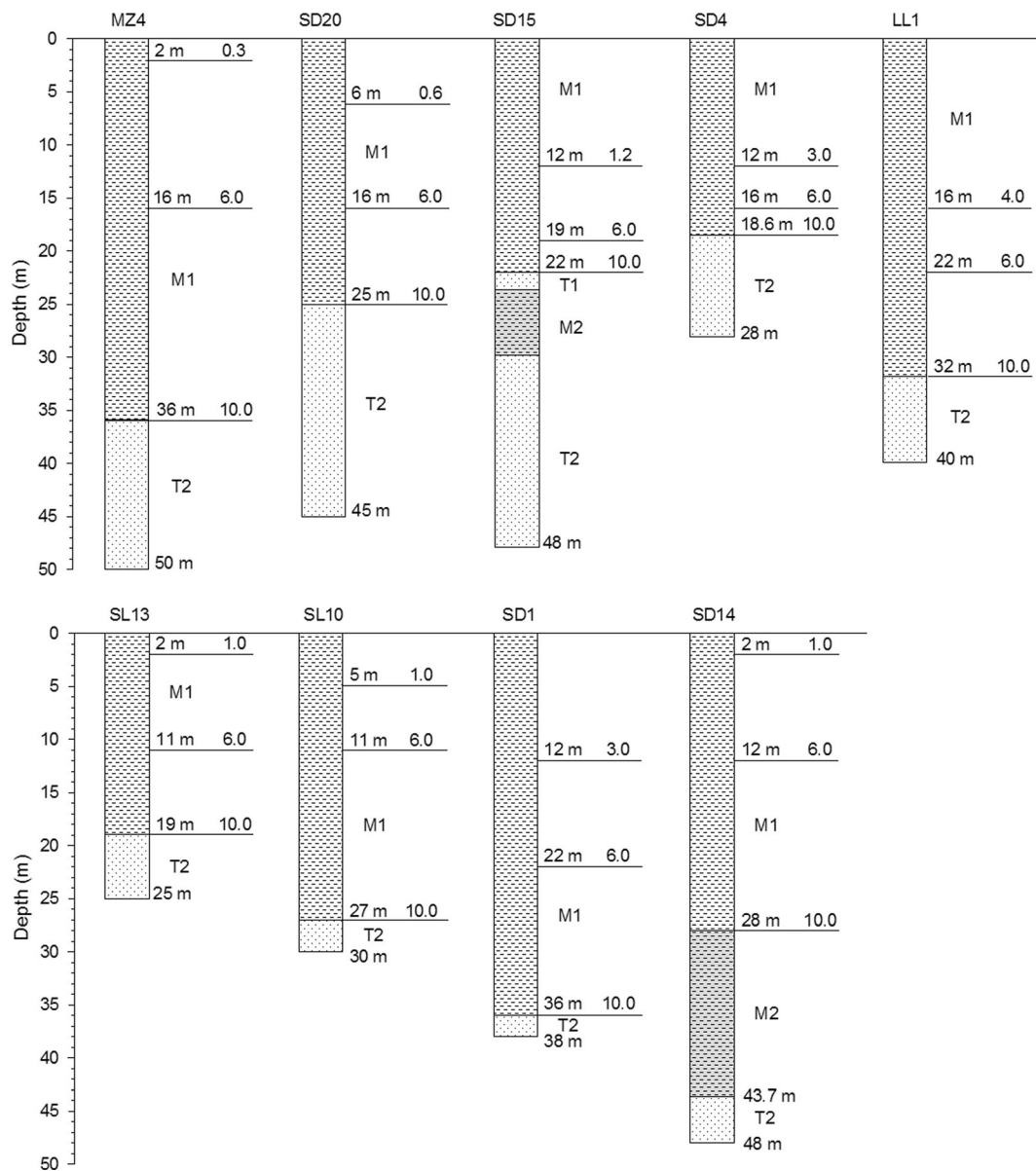


Fig. 2 Schematic of the boreholes with stratigraphic units, borehole depths, and time periods. The numbers on the far right of each log are dates in ka BP. Also shown is the thickness of M1 in each time period

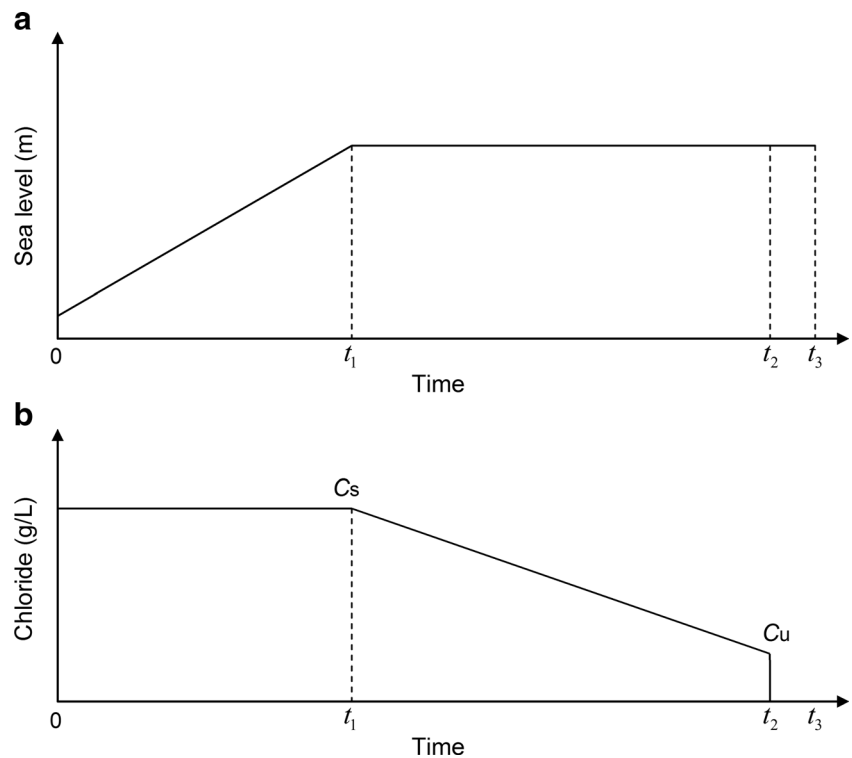
The time t_1 indicates the time at 6 ka BP when the sea level reached the present level. The time t_2 represents the time when the paleo-shoreline passed the location of the borehole and is determined by comparing the positions of the borehole and the paleo-shorelines. The determined t_2 for each borehole is shown in Fig. 2. It can be seen that t_2 ranges from 0.3 to 4.0 ka BP. The time t_3 corresponds to the time at present when the model terminates.

The variations of Cl^- concentration with time at the upper boundary during different periods were determined as follows (Kuang et al. 2015). During the first time period ($0-t_1$), M1 was deposited under seawater and the Cl^- concentration at sediment-water interface (upper boundary) is the Cl^- concentration of the seawater. During the second time period (t_1-t_2),

the seawater became increasingly shallow and the place where a borehole is located changed into a typical situation in an estuary environment. The water above the sediment (M1) may be a mixture of river water and seawater. The Cl^- concentration of the mixed water was assumed to decrease linearly with time during this period. During the third time period (t_2-t_3), the Cl^- concentration at the upper boundary was set to be zero. The upper boundary condition can then be written as (Kuang et al. 2015)

$$C = \begin{cases} C_s, & 0 < t \leq t_1 \\ \frac{C_s - C_u}{t_1 - t_2} t + \frac{C_u t_1 - C_s t_2}{t_1 - t_2}, & t_1 < t \leq t_2 \\ 0, & t_2 < t \leq t_3 \end{cases} \quad (2)$$

Fig. 3 Simplified sea level curve in the PRD and upper boundary conditions (modified from Kuang et al. 2015). **a** Sea level curve in the PRD during the last 10 ka, **b** temporal changes of Cl^- concentration at the upper boundary during the last 10 ka



where C_s is the Cl^- concentration of the seawater and C_u is the Cl^- concentration of the mixed water at t_2 . A schematic of the variations of Cl^- concentration with time at the upper boundary is given in Fig. 3b.

The lower boundary was set to be the surface of the bedrock. Due to the fact that the permeability of the bedrock is much lower than the overlying units, a zero-diffusion flux boundary condition was assumed, which can be expressed as

$$\frac{\partial C}{\partial z} = 0, \quad z = L \quad (3)$$

where L is the depth of the bedrock.

The initial distribution of Cl^- concentration in the units below M1 is unknown. A uniform Cl^- concentration was assumed in all the units below M1 at the time of M1 deposition. The initial condition can be expressed as

$$C = C_0, \quad t = 0 \quad (4)$$

Numerical solution

The mathematical model was solved numerically by using a block-centered upstream finite difference scheme (Kuang et al. 2015). A uniform grid size of $\Delta z = 0.1$ m was set for all the boreholes. In order to reduce error, geometric means of interblock porosities and coefficients of hydrodynamic dispersion were used (Haverkamp and Vauclin 1979; Hornung and

Messing 1983). The Thomas algorithm (Wang and Anderson 1982) was used to solve the resulting linear matrix system.

Sedimentation was simulated by successively adding blocks to the existing model domain (Paul et al. 2001; Schrag et al. 2002; Beekman et al. 2011; Jiao et al. 2015; Kuang et al. 2015). A block with thickness equal to Δz was added to the sediment column when the product of sedimentation rate and simulation time equals Δz . The number of time steps that the model domain moves up, Δz , is calculated as

$$n = \frac{\Delta z}{u \Delta t} \quad (5)$$

where u is the sedimentation rate and Δt is the time step. Sedimentation is continuous and the sedimentation rate in each time period was calculated as the thickness of sediment divided by the sedimentation time. The sedimentation rate is uniform in each time period and it varies in different time periods.

Results and discussion

Chloride concentration profiles

In the model, the thicknesses of M1 at times t_1 and t_2 for each borehole were first specified and then slightly adjusted according to the agreement between simulated and measured data. The determined thickness values are shown in Fig. 2. As t_2 ranges

from 0.3 to 4.0 ka BP, the thickness of M1 during the period from t_2 to t_3 ranges from 2 to 16 m. It is reasonable that the longer the time of sedimentation, the thicker the stratum. Borehole LL1 is the farthest from the sea and it has the thickest M1 during t_2 and t_3 . On the other hand, borehole MZ4 is the nearest to the sea and has the thinnest M1 during t_2 and t_3 .

The calculated sedimentation rates range from 0.65 to 10.00 mm/year (Table 1). Such sedimentation rates compare favorably with previous studies, which range from 0.76 to 40.00 mm/year (Huang et al. 1982; Chen and Luo 1991; Zong et al. 2006; Shi et al. 2010). On the basis of Eq. (5), the time step in each time period can be determined. For each borehole, Δt was set to make sure that n is an integer. The determined Δt for each time period is also listed in Table 1. It can be seen that Δt ranges from 4.65 to 5.71 years. For most of the time periods, Δt is around 5 years.

Initially, the system was assumed to be filled with freshwater and the Cl^- concentration of the freshwater was set to be $C_0 = 0$ (Table 2). This is the case for all the boreholes except MZ4 and SD14. For borehole SD14, the initial Cl^- concentration was set to be $C_0 = 10.0$ g/L because of the thick M2 unit. Zong et al. (2012) shows that SD14 is located in a depositional center. Although the sea level is much lower than the present level at 10 ka BP, some Cl^- could remain in M2 and T2. So, it is reasonable to assume an initial Cl^- concentration in the units below M1 for SD14.

In the simulations, C_s was adjusted according to the agreement between simulated and measured data. Theoretically, C_s should be equal to the Cl^- concentration of standard seawater, i.e., $C_s = 19.0$ g/L. The adjusted values of C_s are shown in Table 2. There are only three boreholes (MZ4, SD14, and SD15) with $C_s = 19.0$ g/L, others are lower than 19.0 g/L. These three boreholes are the deepest ones among the nine boreholes. The lowest C_s is that in SD4, which is only 2.6 g/L. The values of C_s for other boreholes range from 8.8 to 14.0 g/L. Previous studies show that the water salinity distribution in the Pearl River estuary is complicated (Long 1997; Pan et al. 2001; Zong et al. 2010). It is reasonable that the determined C_s value changes

Table 1 Calculated sedimentation rates and time steps

Borehole	u (mm/year)			Δt (years)		
	$0-t_1$	t_1-t_2	t_2-t_3	$0-t_1$	t_1-t_2	t_2-t_3
MZ4	5.00	2.46	6.67	5.00	5.09	5.00
SD20	2.25	1.85	10.00	5.56	5.40	5.00
SD15	0.75	1.46	10.00	5.13	5.27	5.00
SD4	0.65	1.33	4.00	5.13	5.00	5.00
LL1	2.50	3.00	4.00	5.00	5.56	5.00
SL13	2.00	1.80	2.00	5.00	5.05	5.00
SL10	4.00	1.20	5.00	5.00	5.21	5.00
SD1	3.50	3.33	4.00	5.71	5.00	5.00
SD14	4.00	2.00	2.00	5.00	5.00	5.00

Table 2 Initial chloride concentration and chloride concentration at the upper boundary

Borehole	C_0 (g/L)	C_s (g/L)	C_u (g/L)
MZ4	6.7	19.0	2.0
SD20	0	12.5	0
SD15	0	19.0	0
SD4	0	2.6	0
LL1	0	8.8	0
SL13	0	12.0	0
SL10	0	8.8	0
SD1	0	14.0	0
SD14	10.0	19.0	0

with space. Meanwhile, C_u was also determined according to the measured data. The estimated C_u for all the boreholes is 0 except MZ4 (Table 2). The C_u value for MZ4 was chosen to obtain a better fit between simulated and measured data.

A comparison of simulated and measured Cl^- concentration profiles for the nine boreholes is shown in Fig. 4. For each measured profile, the deepest data point represents the Cl^- concentration of groundwater in the basal aquifer. Similar to previous studies, the fit between the simulated and measured Cl^- concentration profiles was visually optimized (Desaulniers et al. 1986; Kuang et al. 2015). Satisfactory agreement was obtained for each borehole. For boreholes SL10 and SL13, the agreement is very good. For MZ4, SD1, and SD14, the measured data are relatively scattered, but the calculated curves represent the general trend of the measured data. A reasonable fit is obtained for each of these boreholes. For boreholes SD20 and SD15, the Cl^- concentration in the aquifer is overestimated and underestimated, respectively. All the simulations were conducted with $\nu = 0$, so $D = D_e$. This means that diffusion solely is adequate to reconstruct the measured Cl^- concentration profiles. The historical transport of Cl^- in the PRD is controlled by diffusion.

The trial and error method was used to estimate the effective diffusion coefficients of the aquitard and aquifer. The initial values of D_e were obtained based on previous studies, which range from 1.0×10^{-11} to 13.1×10^{-10} m²/s (Desaulniers et al. 1981, 1986; Johnson et al. 1989; Eggenkamp et al. 1994; Groen et al. 2000; Hendry et al. 2000; Tokunaga et al. 2011; Wang et al. 2013a; Jiao et al. 2015; Kuang et al. 2015). The estimated D_e of the aquitard ranges from 2.0×10^{-11} m²/s to 2.0×10^{-10} m²/s (Table 3). The estimated D_e of the aquifer ranges from 3.0×10^{-11} m²/s to 4.0×10^{-10} m²/s (Table 3).

The thickness of the aquifer has a significant influence on the Cl^- concentration profiles. When the aquifer is thick, the Cl^- concentration profile shows a subsurface maximum (Fig. 4). The Cl^- concentration first increases with depth, reaches a maximum, and then decreases with

Fig. 4 Comparison of simulated and measured Cl^- concentration profiles for the nine boreholes (measured data from Wang et al. 2013b)

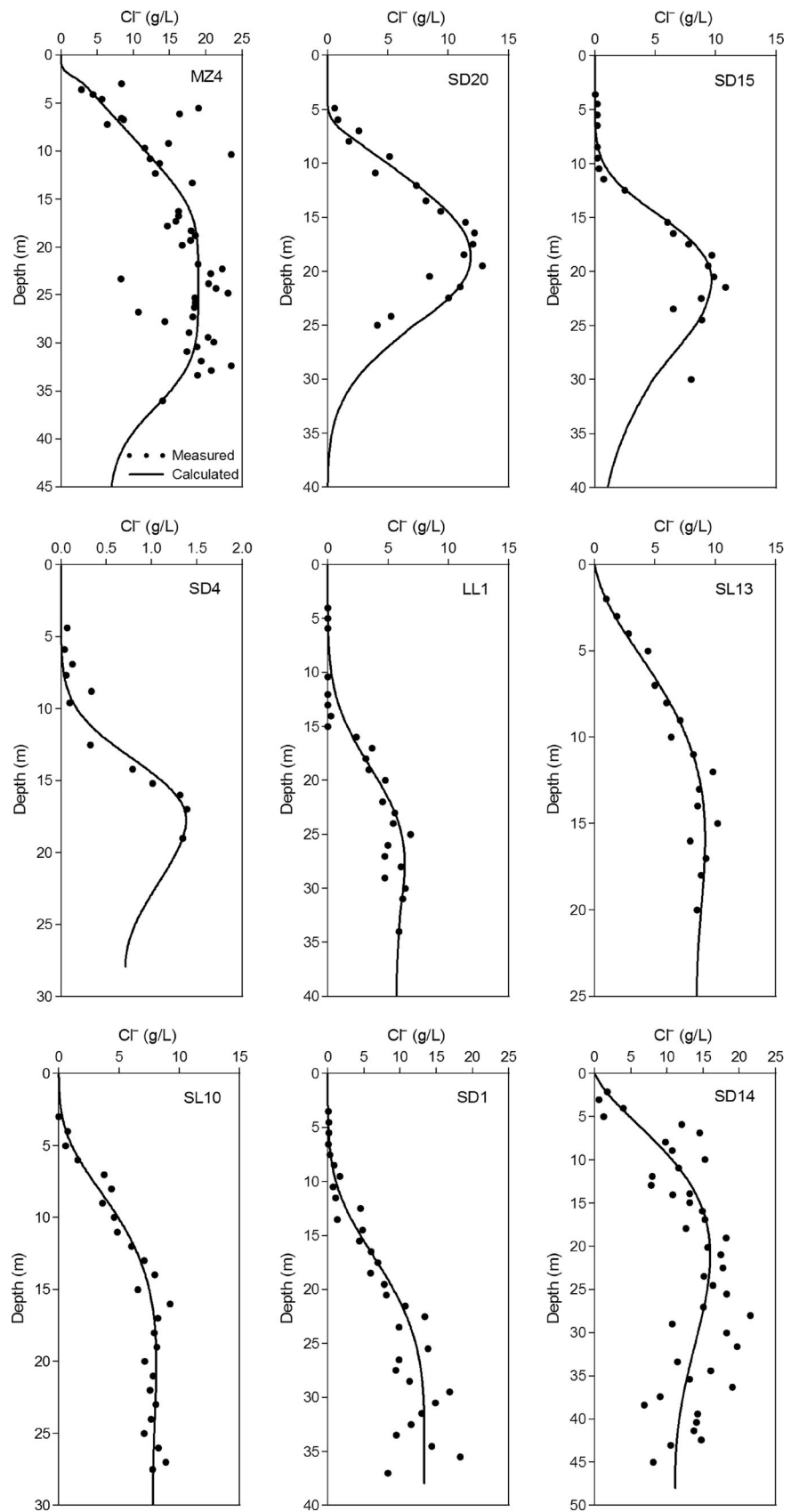


Table 3 Effective diffusion coefficients of the aquitard and the aquifer

Borehole	D_e (m ² /s)	
	Aquitard	Aquifer
MZ4	2.0×10^{-11}	3.0×10^{-11}
SD20	2.0×10^{-11}	4.0×10^{-11}
SD15	1.0×10^{-10}	2.0×10^{-10}
SD4	4.0×10^{-11}	8.0×10^{-11}
LL1	1.0×10^{-10}	3.0×10^{-10}
SL13	1.0×10^{-10}	1.5×10^{-10}
SL10	1.0×10^{-10}	2.0×10^{-10}
SD1	1.0×10^{-10}	2.0×10^{-10}
SD14	2.0×10^{-10}	4.0×10^{-10}

depth. Examples can be seen from boreholes MZ4, SD20, SD15, and SD4. When the aquifer is relatively thin, the Cl^- concentration increases gradually with depth and only a very slight decrease can be seen after the maximum concentration is reached. Examples can be seen from boreholes LL1, SL13, and SL10. Both simulated and measured data show such patterns. For thick aquifers, the diffusion front does not reach the bottom of the aquifer at the end of simulation. So the Cl^- concentration in the lower part of the aquifer is still the initial Cl^- concentration. However, when the aquifer is thin, the diffusion front reaches the bottom of aquifer a short time after the commencement of diffusion and then the Cl^- concentrations of the entire aquifer increase with time.

Historical chloride concentration profiles

The vertical Cl^- concentration distribution at any time of sedimentation can be obtained by the numerical model. Two examples of Cl^- concentration profiles at specified times of sedimentation are shown in Fig. 5. The selected boreholes SD20 and SL13 represent the cases of thick and thin aquifers, respectively. For both cases, the initial Cl^- concentrations were set to be zero. The upper end of each curve at a specified time represents the water-sediment interface or the upper surface of M1 at that time. The curve of 0 ka BP represents the Cl^- concentration profile at present (t_3), which is the curve used to fit the measured data. The evolution of historical Cl^- concentration profiles can be clearly seen in Fig. 5. Such Cl^- concentration profiles will help us to understand the historical Cl^- concentration distributions. At the end of simulations, the diffusion front reaches only about 40 m deep for SD20 because the aquifer is very thick. For SL13, the Cl^- concentration of the groundwater in the aquifer increases from 0 g/L at the start of sedimentation to 8.5 g/L at present.

Sensitivity to effective diffusion coefficient

To illustrate the effect of the effective diffusion coefficient of the aquitard on the simulated Cl^- concentration profiles, different D_e values were chosen for the aquitard and two examples are shown in Fig. 6. Similar to the previous section, boreholes SD20 and SL13 were selected. The results for other boreholes are either similar to SD20 or SL13, depending on the thickness of the aquifer. It can be seen that the distributions of Cl^- concentrations in both the aquitard and the aquifer are affected by different D_e values (Fig. 6). When D_e increases, the Cl^- concentrations in the aquitard tend to be smaller and the Cl^- concentrations in the aquifer tend to be larger. The best fit is obtained when $D_e = 2.0 \times 10^{-11}$ m²/s for SD20 and $D_e = 1.0 \times 10^{-10}$ m²/s for SL13, which is also shown in Fig. 4. The calculated curves significantly underestimated the measured data for the aquitard when $D_e = 8.0 \times 10^{-11}$ m²/s for SD20 and $D_e = 4.0 \times 10^{-10}$ m²/s for SL13. For SD20, the theoretical curves overestimated the Cl^- concentration in the aquifer for all the D_e values. For SL13, the best fit satisfactorily reconstructed the measured data for both the aquitard and the aquifer.

Sensitivity to groundwater flow

Observed groundwater levels in piezometers with different depths show downward hydraulic gradient in the PRD (Jiao et al. 2010; Wang et al. 2013a). To investigate the effect of groundwater flow on the transport of Cl^- , three different downward groundwater velocities (Darcy velocity) were chosen (Fig. 7). The groundwater velocity was only assigned to the period from t_2 to t_3 because, in other periods, the sediment column is under seawater and groundwater velocity was assumed to be 0. The best-fit D_e for both the aquitard and the aquifer were used. The dispersivities of the aquitard and the aquifer were set to be 0.09 and 1.0 m, respectively (Gelhar et al. 1992; Wang et al. 2013a; Kuang et al. 2015).

A comparison of Cl^- concentration profiles for different downward groundwater velocities with the measured profile for boreholes SD20 and SL13 is shown in Fig. 7. For both boreholes, the best fit is obtained when $q=0$. Including a groundwater velocity does not improve the agreement between simulated and measured data. When a groundwater velocity exists, the Cl^- concentrations in the aquitard tend to be underestimated and the Cl^- concentrations in the aquifer tend to be overestimated. This further confirms that the transport of Cl^- in the aquifer–aquitard system in the PRD is controlled by diffusion.

Limitations

The results of this study present an improvement in modeling solute transport in the PRD. The constructed numerical model

Fig. 5 Chloride concentration profiles at different times of sedimentation for boreholes SD20 and SL13

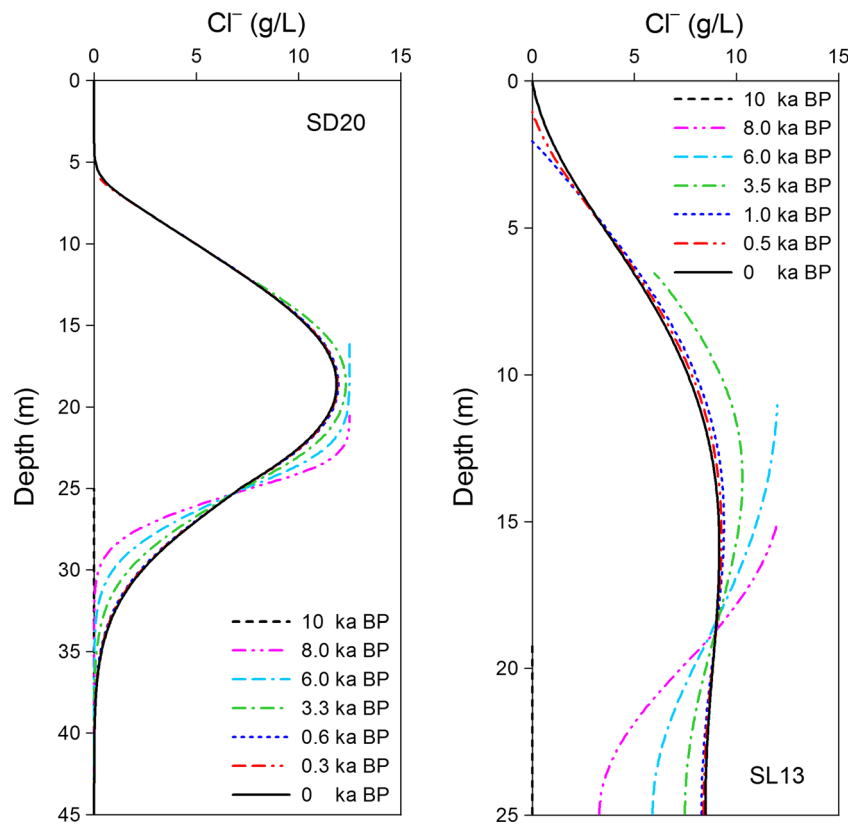


Fig. 6 Comparison of Cl⁻ concentration profiles for different aquitard effective diffusion coefficients for boreholes SD20 and SL13

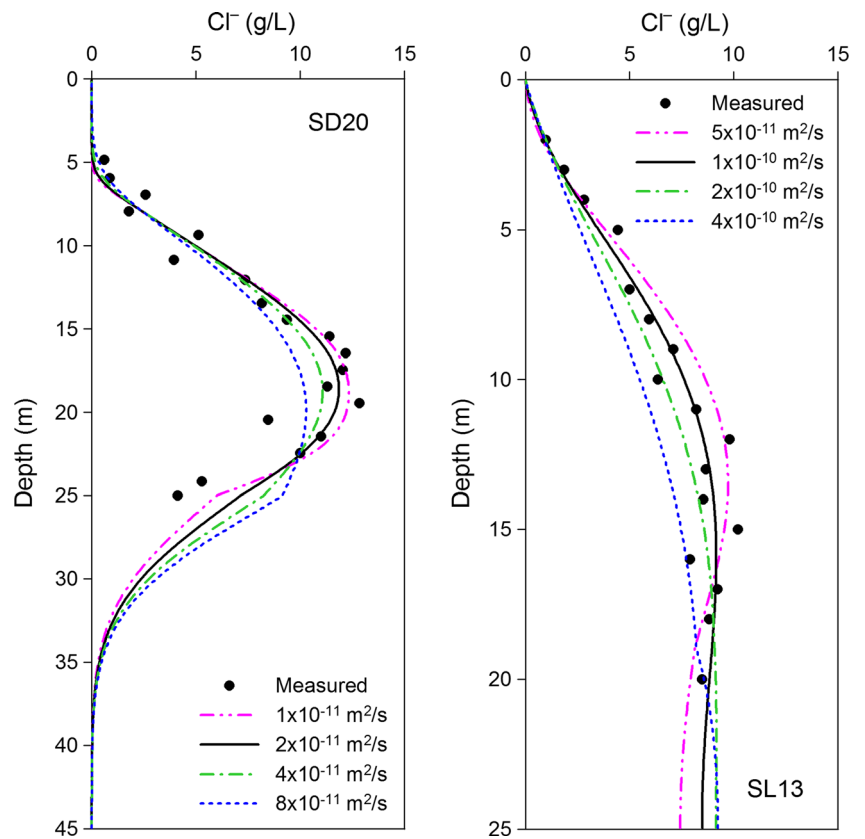
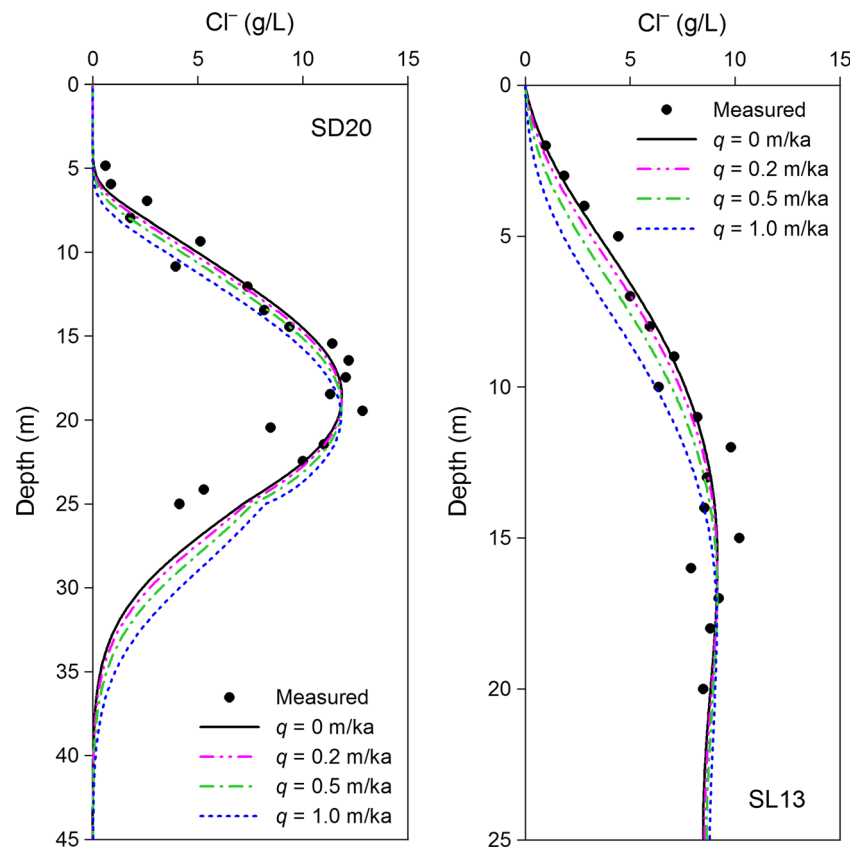


Fig. 7 Comparison of Cl^- concentration profiles for different groundwater velocities for boreholes SD20 and SL13



will also help understand the mechanisms of transport of contaminants in the PRD. Furthermore, this study may be instructive for solute and contaminant transport in other deltas with geological and hydrogeological characteristics similar to the PRD. However, several assumptions and simplifications were used in the model. Density difference was ignored in the model. Compaction-driven groundwater flow was also ignored. The 1D model was used to simulate the measured Cl^- concentration profiles. The model was applied to each of the boreholes and simulated the measured Cl^- concentration profile separately. Lateral advection was not included in the model.

Conclusions

A 1D numerical model is employed to explore the vertical transport mechanisms of Cl^- across a large region of the PRD. The model is constructed based on the sea level changes of the PRD in the Holocene. Sedimentation in the model is continuous and the sedimentation rate varies as the depositional environment in the PRD changes. The model reproduces measured Cl^- concentration profiles in nine boreholes. Overall, satisfactory agreement is obtained between simulated and measured data. In some boreholes, the agreement is very good. The shapes of the simulated Cl^- concentration profiles

are significantly affected by the thickness of the aquifer. Chloride concentration profiles in thick aquifers show a subsurface maximum but Cl^- concentration profiles in thin aquifers do not. Diffusion solely is adequate to reconstruct the Cl^- concentration profiles in all the boreholes. A downward groundwater flow does not improve the agreement between simulated and measured data. The Cl^- concentrations in the aquitard are underestimated and the Cl^- concentrations in the aquifer are overestimated when there is a vertical groundwater flow. The transport of Cl^- in the aquifer–aquitard system in the PRD is controlled by diffusion, and vertical groundwater flow in the areally extensive aquitards is negligible.

The variation of Cl^- concentrations at the upper boundary with time takes into account the evolution of the site from the submarine environment to the terrestrial environment. The goodness of fit between simulated and measured data indicates that the time-dependent upper boundary is applicable across the region. This study helps understand the vertical transport mechanisms of other solutes in the areally extensive aquifer–aquitard system in the PRD. It also improves understanding of time-dependent boundary conditions for solute transport across the region. The model simulations can also be used to improve understanding of the mechanisms of long-term solute transport in other areas with hydrogeological characteristics similar to the PRD.

Acknowledgements The authors thank the associate editor and two anonymous reviewers for their helpful comments. This research was supported by the Research Grants Council of the Hong Kong Special Administrative Region, China (HKU 702612), and an AXA Research Fund Post-Doctoral Fellowship awarded to X.K.

References

- Beekman HE (1991) Ion chromatography of fresh- and seawater intrusion. PhD Thesis, Vrije Universiteit, Amsterdam, The Netherlands
- Beekman HE, Eggenkamp HGM, Appelo CAJ (2011) An integrated modelling approach to reconstruct complex solute transport mechanisms: Cl and $\delta^{37}\text{Cl}$ in pore water of sediments from a former brackish lagoon in The Netherlands. *Appl Geochem* 26(3):257–268
- Chen X, Bao L, Chen J, Zhao X (1990) Discovery of lowest sea level in Late Quaternary at the continental shelf off Pearl River mouth (in Chinese with English abstract). *Trop Oceanol* 9(4):73–77
- Chen X, Huang G, Liang Z (2003) Study on soft soil properties of the Pearl River Delta (in Chinese with English abstract). *Chin J Rock Mech Eng* 22(1):137–141
- Chen Y, Luo Z (1991) Modern sedimentary velocity and their reflected sedimentary characteristics in the Pearl River mouth (in Chinese with English abstract). *Trop Oceanol* 10(2):57–64
- Desaulniers DE, Cherry JA (1989) Origin and movement of groundwater and major ions in a thick deposit of Champlain Sea clay near Montréal. *Can Geotech J* 26(1):80–89
- Desaulniers DE, Cherry JA, Fritz P (1981) Origin, age and movement of pore water in argillaceous Quaternary deposits at four sites in south-western Ontario. *J Hydrol* 50:231–257
- Desaulniers DE, Kaufmann RS, Cherry JA, Bentley HW (1986) ^{37}Cl – ^{35}Cl variations in a diffusion-controlled groundwater system. *Geochim Cosmochim Acta* 50(8):1757–1764
- Eggenkamp HGM (1994) $\delta^{37}\text{Cl}$: the geochemistry of chlorine isotopes. PhD Thesis, Utrecht University, Utrecht, The Netherlands
- Eggenkamp HGM, Middelburg JJ, Kreulen R (1994) Preferential diffusion of ^{35}Cl relative to ^{37}Cl in sediments of Kau Bay, Halmahera, Indonesia. *Chem Geol* 116(3–4):317–325
- Fetter CW (2001) Applied hydrogeology, 4th edn. Prentice-Hall, NJ
- Gelhar LW, Welty C, Rehfeldt KR (1992) A critical review of data on field-scale dispersion in aquifers. *Water Resour Res* 28(7):1955–1974
- Groen J, Velstra J, Meesters AGCA (2000) Salinization processes in paleowaters in coastal sediments of Suriname: evidence from $\delta^{37}\text{Cl}$ analysis and diffusion modelling. *J Hydrol* 234(1–2):1–20
- Harbaugh AW, McDonald MG (1996) User's documentation for MODFLOW-96, an update to the U. S. Geological Survey modular finite-difference ground-water flow model. US Geol Surv Open File Rep 96-485
- Haverkamp R, Vauclin M (1979) A note on estimating finite difference interblock hydraulic conductivity values for transient unsaturated flow problems. *Water Resour Res* 15(1):181–187
- Hendry MJ, Wassenaar LI (1999) Implications of the distribution of δD in pore waters for groundwater flow and the timing of geologic events in a thick aquitard system. *Water Resour Res* 35(6):1751–1760
- Hendry MJ, Wassenaar LI, Kotzer T (2000) Chloride and chlorine isotopes (^{36}Cl and $\delta^{37}\text{Cl}$) as tracers of solute migration in a thick, clay-rich aquitard system. *Water Resour Res* 36(1):285–296
- Hornung U, Messing W (1983) Truncation errors in the numerical solution of horizontal diffusion in saturated/unsaturated media. *Adv Water Resour* 6(3):165–168
- Huang Z, Li P, Zhang Z, Li K, Qiao P (1982) Formation, development, and evolution of the Pearl River Delta (in Chinese). Popular Science Press, Guangzhou, China
- Jiao JJ, Wang Y, Cherry JA, Wang X, Zhi B, Du H, Wen D (2010) Abnormally high ammonium of natural origin in a coastal aquifer–aquitard system in the Pearl River Delta, China. *Environ Sci Technol* 44(19):7470–7475
- Jiao JJ, Shi L, Kuang X, Lee CM, Yim WW-S, Yang S (2015) Reconstructed chloride concentration profiles below the seabed in Hong Kong (China) and their implications for offshore groundwater resources. *Hydrogeol J* 23(2):277–286
- Johnson RL, Cherry JA, Pankow JF (1989) Diffusive contaminant transport in natural clay: a field example and implications for clay-lined waste disposal sites. *Environ Sci Technol* 23(3):340–349
- Kuang X, Jiao JJ, Liu K (2015) Numerical studies of vertical Cl^- , $\delta^2\text{H}$ and $\delta^{18}\text{O}$ profiles in the aquifer–aquitard system in the Pearl River Delta, China. *Hydrol Process* 29(19):4199–4209
- Lan X (1991) Sedimentary characteristics and strata division of core $\Delta 22$ of the Zhujiang River Delta (in Chinese with English abstract). *Oceanol Limnol Sin* 22(2):148–154
- Li P, Qiao P (1982) The model of evolution of the Pearl River Delta during last 6,000 years (in Chinese with English abstract). *J Sediment Res* 3:33–42
- Li P, Qiao P, Zheng H, Fang G, Huang G (1991) The environment evolution of the Zhujiang Delta in the last 10,000 years (in Chinese). China Ocean Press, Beijing
- Long Y (1997) Sediment geology of the Pearl River Delta (in Chinese). Geological Publishing House, Beijing
- McDonald MG, Harbaugh AW (1988) A modular three-dimensional finite-difference ground-water flow model. Techniques of Water-Resources Investigations, Book 6, Chapter A1, US Geological Survey, Reston, VA
- Middelburg JJ, de Lange GJ (1989) The isolation of Kau Bay during the last glaciation: direct evidence from interstitial water chlorinity. *Neth J Sea Res* 24(4):615–622
- Neuzil CE (1986) Groundwater flow in low-permeability environments. *Water Resour Res* 22(8):1163–1195
- Ogata A, Banks RB (1961) A solution of the differential equation of longitudinal dispersion in porous media. *US Geol Surv Prof Pap* 411-A
- Pan J, Zhou H, Liu X, Hu C, Dong L, Zhang M (2001) Nutrient profiles in interstitial water and flux in water-sediment interface of the Zhujiang Estuary of China in summer. *Acta Oceanol Sin* 20(4):523–533
- Paul HA, Bernasconi SM, Schmid DW, McKenzie JA (2001) Oxygen isotopic composition of the Mediterranean Sea since the Last Glacial Maximum: constraints from pore water analyses. *Earth Planet Sci Lett* 192(1):1–14
- Schrag DP, Adkins JF, McIntyre K, Alexander JL, Hodell DA, Charles CD, McManus JF (2002) The oxygen isotopic composition of seawater during the Last Glacial Maximum. *Quat Sci Rev* 21(1–3):331–342
- Shi Q, Leipe T, Rueckert P, Zhou D, Harff J (2010) Geochemical sources, deposition and enrichment of heavy metals in short sediment cores from the Pearl River Estuary, southern China. *J Mar Syst* 82:S28–S42
- Tokunaga T, Shimada J, Kimura Y, Inoue D, Mogi K, Asai K (2011) A multiple-isotope ($\delta^{37}\text{Cl}$, ^{14}C , ^3H) approach to reveal the coastal hydrogeological system and its temporal changes in western Kyushu, Japan. *Hydrogeol J* 19(1):249–258
- van der Kamp G, Van Stempvoort DR, Wassenaar LI (1996) The radial diffusion method: 1, using intact cores to determine isotopic composition, chemistry, and effective porosities for groundwater in aquitards. *Water Resour Res* 32(6):1815–1822
- Wang Y (2011) Isotopic and hydrogeochemical studies of the coast aquifer–aquitard system in the Pearl River Delta, China. PhD Thesis, The University of Hong Kong, Hong Kong
- Wang HF, Anderson MP (1982) Introduction to groundwater modeling: finite difference and finite element methods. Academic, San Diego, CA

- Wang Y, Jiao JJ (2012) Origin of groundwater salinity and hydrogeochemical processes in the confined Quaternary aquifer of the Pearl River Delta, China. *J Hydrol* 438–439:112–124
- Wang Y, Jiao JJ, Cherry JA (2012) Occurrence and geochemical behavior of arsenic in a coastal aquifer–aquitarde system of the Pearl River Delta, China. *Sci Total Environ* 427–428:286–297
- Wang X-S, Jiao JJ, Wang Y, Cherry JA, Kuang X, Liu K, Lee C, Gong Z (2013a) Accumulation and transport of ammonium in aquitards in the Pearl River Delta (China) in the last 10,000 years: conceptual and numerical models. *Hydrogeol J* 21(5):961–976
- Wang Y, Jiao JJ, Cherry JA, Lee CM (2013b) Contribution of the aquitarde to the regional groundwater hydrochemistry of the underlying confined aquifer in the Pearl River Delta, China. *Sci Total Environ* 461–462:663–671
- Wei X, Wu C (2011) Holocene delta evolution and sequence stratigraphy of the Pearl River Delta in South China. *Sci China Earth Sci* 54(10): 1523–1541
- Wu CY, Ren J, Bao Y, Lei YP, Shi HY (2007) A long-term morphological modeling study on the evolution of the Pearl River Delta, network system, and estuarine bays since 6000 yr B.P. In: *Coastline changes: interrelation of climate and geological processes*. In: Harff J, Hay WW, Tetzlaff DM, Harff J, Hay WW, Tetzlaff DM (eds) *The Geological Society of America Special Paper 426*. GSA, Boulder, CO, pp 199–214
- Yang H, Xie Z (1985) Sea-level changes and climatic fluctuations over the last 20,000 years in China (in Chinese). In: *Contribution to the Quaternary glaciology and Quaternary geology*, vol 2. Geological Publishing House, Beijing
- Yang L, Wang X-S, Jiao JJ (2015) Numerical modeling of slug tests with MODFLOW using equivalent well blocks. *Ground Water* 53(1): 158–163
- Yim WW-S, Huang G, Fontugne MR, Hale RE, Paterne M, Pirazzoli PA, Ridley Thomas WN (2006) Postglacial sea-level changes in the northern South China Sea continental shelf: evidence for a post-8200 calendar yr BP meltwater pulse. *Quat Int* 145–146:55–67
- Zheng C (1990) MT3D: a modular three-dimensional transport model for simulation of advection, dispersion and chemical reaction of contaminants in groundwater systems. Report to the US Environmental Protection Agency, Robert S Kerr Environmental Research Laboratory, Ada, OK
- Zheng C, Bennett GD (2002) *Applied contaminant transport modeling*, 2nd edn. Wiley, New York
- Zong Y (2004) Mid-Holocene sea-level highstand along the southeast coast of China. *Quat Int* 117(1):55–67
- Zong Y, Lloyd JM, Leng MJ, Yim WW-S, Huang G (2006) Reconstruction of Holocene monsoon history from the Pearl River Estuary, southern China, using diatoms and carbon isotope ratios. *The Holocene* 16(2):251–263
- Zong Y, Huang G, Switzer AD, Yu F, Yim WW-S (2009a) An evolutionary model for the Holocene formation of the Pearl River delta, China. *The Holocene* 19(1):129–142
- Zong Y, Yim WW-S, Yu F, Huang G (2009b) Late Quaternary environmental changes in the Pearl River mouth region, China. *Quat Int* 206(1–2):35–45
- Zong Y, Yu F, Huang G, Lloyd JM, Yim WW-S (2010) The history of water salinity in the Pearl River estuary, China, during the Late Quaternary. *Earth Surf Process Landf* 35(10):1221–1233
- Zong Y, Huang K, Yu F, Zheng Z, Switzer A, Huang G, Wang N, Tang M (2012) The role of sea-level rise, monsoonal discharge and the palaeo-landscape in the early Holocene evolution of the Pearl River delta, southern China. *Quat Sci Rev* 54:77–88